

EXACT FULLY 3D NAVIER–STOKES SOLUTIONS FOR BENCHMARKING

C. ROSS ETHIER AND D. A. STEINMAN

Department of Mechanical Engineering, 5 King's College Road, University of Toronto, Toronto, Ontario M5S 1A4, Canada

SUMMARY

Unsteady analytical solutions to the incompressible Navier–Stokes equations are presented. They are fully three-dimensional vector solutions involving all three Cartesian velocity components, each of which depends non-trivially on all three co-ordinate directions. Although unlikely to be physically realized, they are well suited for benchmarking, testing and validation of three-dimensional incompressible Navier–Stokes solvers. The use of such a solution for benchmarking purposes is described.

KEY WORDS Navier–Stokes equations Incompressible Three-dimensional Exact solution Benchmarking Penalty formulation

1. INTRODUCTION

Development and testing of Navier–Stokes solvers are facilitated by comparison of numerical results with benchmarks. Benchmarks can be exact (analytic) solutions to the Navier–Stokes equations,^{1,2} high-resolution numerical simulations (see e.g. References 3 and 4) or reliable experimental data sets. Each of these possibilities has drawbacks. For example, many exact solutions of the Navier–Stokes equations are degenerate in the sense that certain terms in the governing equations are identically zero. This precludes testing of all aspects of the numerical algorithm, e.g. interactions between convective terms and a Stokes solver in a split step approach. To the best of our knowledge there are no exact closed-form solutions which involve all terms in the Navier–Stokes equations and are fully three-dimensional.² High-resolution numerical benchmark simulations, while common for two-dimensional (2D) flows, are extremely expensive for fully 3D Navier–Stokes flows. Although 3D solvers can of course be used to simulate 2D flows, debugging and complete evaluation of 3D code performance is best provided by full 3D flows. Finally, experimental data sets can contain measurement errors that complicate validation studies.

In this work we consider analytical benchmarks and seek to develop ‘full’ solutions to the incompressible 3D Navier–Stokes equations. Such solutions should have non-zero (and non-trivial) velocities in each of the three co-ordinate directions. Further, each velocity component should depend on all three spatial co-ordinates (x , y , z), should be expressible in closed form, and should be such that the unsteady, convective, pressure and diffusive terms in the Navier–Stokes equations are all non-zero.

Development of a 3D solution was motivated by an exact 2D solution originally derived by Taylor:⁵

$$u = -\cos(\pi x)\sin(\pi y)e^{-2\pi^2\nu t}, \quad (1a)$$

$$v = \sin(\pi x)\cos(\pi y)e^{-2\pi^2\nu t}, \quad (1b)$$

$$p = -\frac{\cos(2\pi x) + \cos(2\pi y)}{4} e^{-4\pi^2\nu t}, \quad (1c)$$

where (u, v) are the velocity components in the (x, y) -directions. Equations (1) constitute a 2D Navier–Stokes solution in which the unsteady terms balance the diffusive terms, while the convective terms balance the pressure gradient, and have been used for 2D benchmarking.⁶

2. METHODS

We search for an exact solution to the 3D Navier–Stokes equations in Cartesian co-ordinates, written here in dimensionless form:

$$\partial\mathbf{v}/\partial t + Re \mathbf{v} \cdot \nabla\mathbf{v} = -Re \nabla p + \nabla^2\mathbf{v}, \quad (2)$$

$$\nabla \cdot \mathbf{v} = 0, \quad (3)$$

where $Re = UL/\nu$ and the following characteristic quantities are defined: length L , velocity U , time L^2/ν and pressure ρU^2 . Motivated by Taylor's 2D solution, we construct a velocity field \mathbf{v} such that

- (1) unsteady terms balance viscous terms in the momentum equations
- (2) the velocity field is divergence-free
- (3) the convective terms $\mathbf{v} \cdot \nabla\mathbf{v}$ can be expressed as the gradient of a scalar function (the negative of the pressure).

In order to satisfy the first criterion, we assume a separable solution of the form

$$\mathbf{v}(x, t) = \mathbf{V}(\mathbf{x})T(t), \quad (4)$$

with

$$dT/dt = \lambda^2 T, \quad (5a)$$

$$\nabla^2\mathbf{V} = \lambda^2\mathbf{V}. \quad (5b)$$

Equation (5a) requires that $T(t) = e^{\lambda^2 t}$.

The second criterion can be satisfied by use of a (vector-valued) generalization of the streamfunction Ψ such that $\mathbf{V} = \nabla \times \Psi$. Equation (5b) implies that Ψ must satisfy

$$\nabla^2\Psi = \lambda^2\Psi. \quad (6)$$

We construct Ψ via

$$\Psi = \mathbf{i}\Psi_{yz} + \mathbf{j}\Psi_{zx} + \mathbf{k}\Psi_{xy}, \quad (7)$$

where Ψ_{yz} , Ψ_{zx} and Ψ_{xy} are scalar functions of the form

$$\Psi_{yz} = f(y)g(z)h(x), \quad (8)$$

$$\Psi_{zx} = f(z)g(x)h(y), \quad (9)$$

$$\Psi_{xy} = f(x)g(y)h(z), \quad (10)$$

\mathbf{i} , \mathbf{j} and \mathbf{k} are Cartesian basis vectors and f , g and h are arbitrary functions. In order to satisfy (6), we require

$$f'' = a^2 f, \quad (11a)$$

$$g'' = b^2 g, \quad (11b)$$

$$h'' = c^2 h, \quad (11c)$$

with $\lambda^2 = a^2 + b^2 + c^2$.

It remains to satisfy the third criterion, for which a necessary and sufficient condition is that the curl of $\mathbf{v} \cdot \nabla \mathbf{v}$ vanish. Using standard vector identities, this condition can be rewritten as

$$\nabla \times (\mathbf{V} \times (\nabla \times \mathbf{V})) = \mathbf{0}. \quad (12)$$

If this condition holds, the pressure is given by

$$p = -\frac{1}{2}(\mathcal{R}\{\mathbf{V}\} \cdot \mathcal{R}\{\mathbf{V}\} + H)T^2(t), \quad (13)$$

where H is a function which satisfies $\nabla H = -2\mathcal{R}\{\mathbf{V}\} \times (\nabla \times \mathcal{R}\{\mathbf{V}\})$ and $\mathcal{R}\{\cdot\}$ is the real part of a quantity. Flows which satisfy (12) are the so-called generalized Beltrami flows.¹ A sufficient condition for (12) to hold is $\mathbf{V} \times (\nabla \times \mathbf{V}) = \mathbf{0}$, in which case the flow is said to be a Beltrami or Trkal flow.^{1,2} We must choose f , g and h such that (12) is satisfied.

We note in passing that Taylor's 2D flow is obtained by setting $\Psi_{yz} = \Psi_{zx} = 0$ and $h = 1$, in which case $\Psi_{xy} = f(x)g(y)$. In this case $\nabla \cdot \Psi = 0$ and (12) will always hold.

3. RESULTS

By virtue of condition (11), the functions f , g and h must be either sines, cosines, exponential or constant functions or linear combinations thereof. We consider several possible combinations below.*

3.1. f , g and h exponentials

Condition (11) requires that $f(x) = e^{ax}$, $g(x) = e^{bx}$ and $h(x) = e^{cx}$. Equations (12) are non-trivially satisfied by the following combinations of (a, b, c) .

- (1) $a + b + c = 0$ for (a, b, c) all real. This is a generalized Beltrami flow and yields the following velocity and pressure fields:

$$u = (be^{a(x-z)+b(y-z)} - ae^{a(z-y)+b(x-y)})e^{[a^2+b^2+(a+b)^2]t}, \quad (14a)$$

$$v = (be^{a(y-x)+b(z-x)} - ae^{a(x-z)+b(y-z)})e^{[a^2+b^2+(a+b)^2]t}, \quad (14b)$$

$$w = (be^{a(z-y)+b(x-y)} - ae^{a(y-x)+b(z-x)})e^{[a^2+b^2+(a+b)^2]t}, \quad (14c)$$

$$p = (a^2 + b^2 + ab)(e^{a(x-y)+b(x-z)} + e^{a(y-z)+b(y-x)} + e^{a(z-x)+b(z-y)})e^{2[a^2+b^2+(a+b)^2]t}, \quad (14d)$$

where a and b are real constants. Although benchmarking with this solution is possible, it is less than ideal, since the exponential temporal growth of the solution may mask numerical instabilities.

* Note that an exhaustive analysis of all possible combinations was not made and the above formulation may admit more exact solutions than presented here.

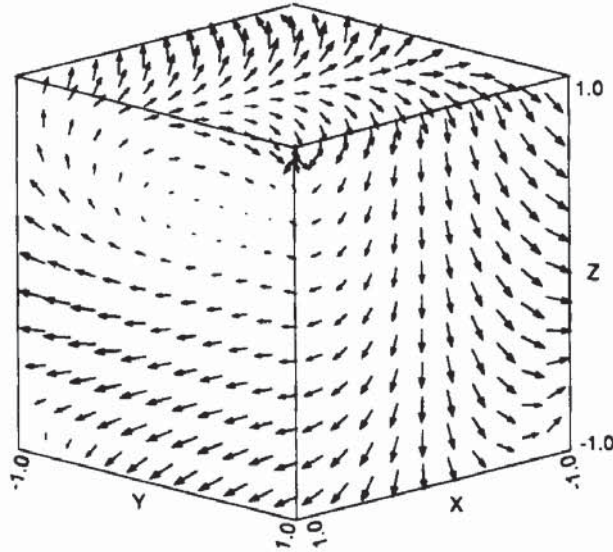


Figure 1. Vector plot of flow field defined by (15) for $a = \pi/4$ and $d = \pi/2$ at time $t = 0$. Three-dimensional velocity vectors on three sides of the unit cube corresponding to $x = 1$, $y = 1$ and $z = 1$ are plotted

- (2) $a^2 + b^2 = 0$, c pure imaginary. This is a Beltrami flow and yields a family of velocity and pressure fields depending on the selection of a and b . If a is chosen to be real so that $b = \pm ia$ and c is written as $c = id$ for d real and arbitrary, then the following solutions are obtained:

$$u = -a[e^{ax} \sin(ay \pm dz) + e^{az} \cos(ax \pm dy)]e^{-d^2t}, \quad (15a)$$

$$v = -a[e^{ay} \sin(az \pm dx) + e^{ax} \cos(ay \pm dz)]e^{-d^2t}, \quad (15b)$$

$$w = -a[e^{az} \sin(ax \pm dy) + e^{ay} \cos(az \pm dx)]e^{-d^2t}, \quad (15c)$$

$$p = -\frac{a^2}{2} [e^{2ax} + e^{2ay} + e^{2az} + 2 \sin(ax \pm dy)\cos(az \pm dx)e^{a(y+z)} + 2 \sin(ay \pm dz)\cos(ax \pm dy)e^{a(z+x)} + 2 \sin(az \pm dx)\cos(ay \pm dz)e^{a(x+y)}]e^{-2d^2t}. \quad (15d)$$

Equations (15) result from taking the real part of \mathbf{V} . A second solution, found by taking the imaginary part of \mathbf{V} , has a form identical to (15), except that (i) for the case $b = ia$ cosines are replaced by sines and sines are replaced by negative cosines and (ii) for the case $b = -ia$ cosines are replaced by negative sines and sines are replaced by cosines.* The above solution appears to be well suited to benchmarking, since it decays exponentially in time. A portion of this flow field is shown in Figure 1. Although the fully 3D structure of the flow is difficult to visualize, it seems to consist of a series of counter-rotating vortices intersecting one another at oblique angles. For the parameter values used to generate Figure 1, only a portion of a vortex falls within the plotted domain.

* A second, closely related family of solutions is obtained by choosing a to be purely imaginary and b real. They are not reproduced herein so as to conserve space.

3.2. f , g and h combinations of sine, cosine, sinh and cosh

Solutions of the above form were only found when h was set equal to one. In this case four solutions with $f(x) = \cosh(bx)$ or $\sinh(bx)$ and $g(y) = \sin(by)$ or $\cos(by)$ were found. These are steady Beltrami flows which are inviscid solutions to the Navier–Stokes equations. They are therefore not suitable for benchmarking full Navier–Stokes solvers.

4. NUMERICAL TESTING

A well-validated finite element solver⁷ was used to demonstrate the use of the above analytic solution for benchmarking. The solver uses Galerkin spatial discretization of the 3D unsteady Navier–Stokes equations, with modified Crouzeix–Raviart Q_2 – P_1 brick elements⁸ and second-order implicit Gear time marching. The convective terms were treated implicitly using Newton linearization, while the pressure was decoupled from the momentum equation using the penalty formulation.⁸ This code is expected to demonstrate $O(h^3)$ spatial accuracy in velocity, $O(h^2)$ spatial accuracy in pressure and $O(\Delta t^2)$ temporal accuracy, where h is a measure of mesh size.

A cube centred at $(0, 0, 0)$ and extending one unit in all directions was used for the tests. This domain was discretized uniformly with 2–7 brick elements (i.e. $h = 0.5$ – 0.14 , where h is the space between adjacent nodes per direction. In all tests the independent constants in equations (15) were chosen as $a = \pi/4$ and $d = \pi/2$, resulting in initial velocities ranging from 1.59 to -3.31 and a 22% decay after time $t = 0.1$. These values were chosen to optimize spatial and temporal variation while maintaining reasonable execution times and are identical to those used to plot Figure 1. Numerical solutions were computed by specifying an initial ($t = 0$) velocity field everywhere via equations (15) and stepping a specified number of time steps to $t = 0.1$. Dirichlet boundary conditions, also based upon equations (15), were applied on all faces. The velocity

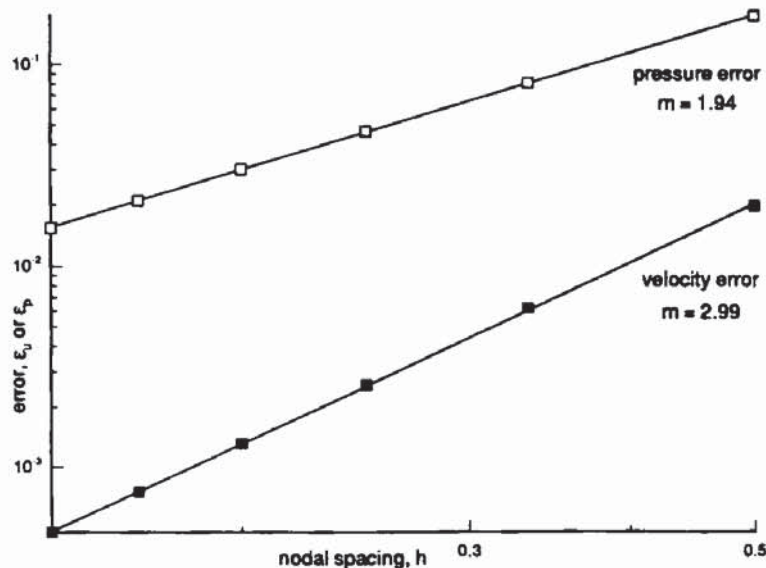


Figure 2. Plot of velocity (ϵ_v) and pressure (ϵ_p) errors versus node spacing (h) for the analytic flow field as computed by the penalty finite element code described in the text. Data points were obtained for meshes with 2–7 elements per co-ordinate direction, solid lines are the least-squares linear fit to the logarithmic data and m is the slope of the corresponding fitted line. Sixteen time steps were used to step to $t = 0.1$ to ensure that the temporal error was small for all tests, and $Re = 1$ for this set of runs

field at time $t = 0.1$ was compared against the analytic field using a 'normalized L_2 difference norm' or ε_u defined as

$$\varepsilon_u = \|\mathbf{u} - \mathbf{u}_{\text{exact}}\|_{L_2} / \|\mathbf{u}_{\text{exact}}\|_{L_2}, \quad (16)$$

where \mathbf{u} is the numerically computed velocity field, $\mathbf{u}_{\text{exact}}$ is the analytic velocity field and $\|\cdot\|_{L_2}$ is the standard L_2 -norm. A similar error measure ε_p , was computed at $t = 0.1$ for the pressure. All L_2 -norms were computed elementwise using Gaussian quadrature of sufficiently high order as to match the analytical and numerical values for $\|\mathbf{u}_{\text{exact}}\|_{L_2}$ to within machine accuracy.

Figure 2 shows computed velocity (ε_u) and pressure (ε_p) errors as a function of nodal spacing h for the domain and flow field described above. Meshes with 2–7 elements per dimension were used to obtain the data points shown. The slope of the lines regressed to these data confirms the $O(h^3)$ and $O(h^2)$ performance of the code for the velocity and pressure interpolations respectively.

5. DISCUSSION

Although the flow defined by (15) will likely never be physically realized, it is an excellent numerical benchmark/test case for several reasons. First, since closed-form expressions for the velocities and pressure are known, individual terms in the Navier–Stokes equations can be analytically computed and compared with their numerical counterparts. We have found this capability to be very helpful for debugging purposes. Secondly, this solution can be imposed on arbitrarily shaped finite domains, permitting effects of mesh distortion to be quantified. Thirdly, this solution is valid for all Reynolds numbers, so that the effects of Re on the solver can be assessed simply. Fourthly, as can be seen from Figure 1, the flow field is rather complex and is not unidirectional, thus providing a 'challenging' test case. Finally, although the solution is constructed so that unsteady and diffusive terms balance, as do convective and pressure gradient terms, the numerical solver does not 'know' that this is the case. Thus (15) provides a robust test for a solver.

A potential problem in use of the above analytic solution for benchmarking is the application of boundary conditions. Imposition of Dirichlet conditions at every boundary has the potential to lead to 'wiggles' in the velocity field near the boundary. This problem can be partially alleviated by specification of non-homogeneous Neumann conditions at some boundaries. However, it is prudent to check for the existence of such disturbances before using calculated velocity fields as the basis of error estimates. The presence of such wiggles would indicate that the grid Peclet number near the boundary should be reduced, either through use of higher spatial resolution or lower Reynolds numbers. In practice, for tests with $Re = 1, 10$ or 100 no wiggles were observed in computed velocity fields, with the exception of runs at $Re = 100$ with three or fewer elements per co-ordinate direction. These coarse mesh runs at $Re = 100$ failed to converge, probably owing to the growth of boundary-induced wiggles.

The above solution is not intended to replace other standard benchmarks such as the driven cavity problem or flow over a backward facing step. However, it should prove useful as an additional benchmarking tool in the development of 3D incompressible Navier–Stokes solvers.

ACKNOWLEDGEMENTS

Helpful comments from Steve Karpik are gratefully acknowledged. This work was supported in part by a grant from the Whitaker Foundation and by Canadian NSERC grant A2191.